International Journal of Microwave and Wireless Technologies, 2013, 5(6), 659–667.
doi:10.1017/S1759078713000688

RESEARCH PAPER

Comparative analysis of receiver bandwidth effects on Y-factor and cold-source noise figure measurements

NEREA OTEGI[1], JUAN-MARI COLLANTES[1] AND MOHAMED SAYED[2]

A known source of error in noise figure characterization is the variation of the device characteristics within the bandwidth of the instrument receiver. In this paper, an in-depth analysis of the effect of the receiver bandwidth on noise figure characterization accuracy is developed. For the first time, comparative results for Y-factor and cold-source techniques are given. The analysis clarifies some contradictions about the origin and the final impact of bandwidth effects in Y-factor. In addition, effects derived from an excessively wide bandwidth of the noise receiver are shown to be completely different in both techniques, being more critical in cold-source. As a result of the analysis, correction terms are provided for those cases in which receivers with narrow enough bandwidths are not available. The conclusions extracted from the theoretical formulation are confirmed by the measurements carried out on several narrow-band devices under tests with different characteristics.

Keywords: Microwave measurements, Modeling, Simulation and characterizations of devices and circuits, Noise figure measurement

Received 14 January 2013; Revised 15 May 2013; first published online 8 July 2013

I. INTRODUCTION

Accurate noise characterization of radio frequency (RF) and microwave devices is an essential part in the process of developing performance receivers for modern wireless communications. Measurement accuracy in different noise characterization processes has been widely treated in the literature, with special focus on mismatch derived effects [1–13]. Traditionally, noise figure measurements of circuits and subsystems were typically performed using the Y-factor technique [14–16]. Nonetheless, cold-source technique, mainly used to compute device noise parameters in the past [17–21], is being increasingly used in modern equipment for noise figure characterization [22, 23]. Regardless of the technique used, the bandwidth of the noise receiver is an additional source of error in noise figure characterization when device under test (DUT) characteristics vary within this bandwidth. When performing a noise measurement at a certain frequency, the noise receiver measures the overall noise power within its noise bandwidth. Typically, this bandwidth should be narrow enough for the DUT characteristics to remain unchanged. The noise figure computed will then agree with the desired noise figure at measurement frequency, i.e. the spot noise figure [24] at that frequency. However, there are circumstances in which the DUT presents significant variations within the bandwidth of the receiver. This can happen either because the DUT is ultra narrow-band or just because a relatively large receiver bandwidth is imposed by the capabilities of the instrument or by the need of speeding up the measurement process. As an example, the narrowest bandwidth of some modern instruments with noise figure measurement capabilities is 800 kHz [25]. This may not be narrow enough for accurate measurement at the pass-band edge of a DUT with a very sharp roll-off.

While it is well known that the bandwidth of the noise receiver has to be narrower than the bandwidth of the DUT in order to avoid inaccuracies [26–28], the effect of the opposite situation is not completely clear and contradictory results can be found [28–32]. Only Y-factor based measurements were considered in [28–32].

In this paper, a comparative analysis of bandwidth effects on Y-factor and cold-source noise figure measurements is performed. The analysis is founded on a full theoretical formulation that serves to explain the origin and assess the impact of these effects on both techniques. As will be shown in this work, errors associated with bandwidth effects in cold-source are completely different from Y-factor. Moreover, they are more critical and difficult to avoid, since they are not negligible for high gain DUTs as occurs with Y-factor. As an outcome of the analysis, corrections are proposed to minimize bandwidth errors whenever relevant. All the conclusions are confirmed and validated by measurements performed on different DUTs.

The paper is organized as follows. In Section II, the bases of Y-factor and cold-source noise figure measurement techniques are summarized. General expressions of Y-factor and cold-source based noise figure measurements as a function

[1]Electricity and Electronics Department, University of the Basque Country (UPV/EHU), Apdo. 644, 48080 Bilbao, Spain. Phone: + 34 946015944
[2]Microwave&Millimeter Wave Solutions, Santa Rosa, CA 95404, USA
Corresponding author:
N. Otegi
Email: nerea.otegi@ehu.es

of spot noise figure and gain values are given in Section III. An analytical study of bandwidth effects when system bandwidth is limited by the DUT during the measurement process is then developed in Section IV. Correction terms are proposed in Section V to improve accuracy when narrow-band receivers are not available. Finally, in Section VI, experimental results from various DUTs are provided to confirm the conclusions extracted from the analysis and to verify the validity of the correction terms.

II. FUNDAMENTALS ON Y-FACTOR AND COLD-SOURCE NOISE FIGURE MEASUREMENT TECHNIQUES

The noise figure of a two-port is defined in [24] as the ratio between the total noise power available at the output port per unit bandwidth and the contribution to this noise exclusively coming from the source termination, which can be written as:

$$F(f) = \frac{N_o(f)}{G_{av}(f)kT_o}, \tag{1}$$

where $N_o(f)$ is the noise power available per unit bandwidth at the output port, k is the Boltzmann constant, T_o is the standard reference temperature of 290 K, and $G_{av}(f)$ is the available gain of the two-port, given in (2).

$$G_{av}(f) = \frac{(1-|\Gamma_s|^2)}{|1-s_{11}\Gamma_s|^2}|s_{21}|^2\frac{1}{(1-|\Gamma_{out}|^2)}, \tag{2}$$

$\boldsymbol{S}_{ij}$ being the S-parameters of the two-port, $\boldsymbol{\Gamma}_{out}$ its output reflection coefficient, and $\boldsymbol{\Gamma}_s$ is the source reflection coefficient.

To emphasize that the noise figure (1) is a point function of frequency, the term spot noise figure is used in [24].

The Y-factor and the cold-source techniques are the two main noise figure measurement techniques. The bases of these two techniques are widely reported in the literature [17–19, 24, 33, 34]. Some fundamentals on these procedures are summarized here.

A) Y-factor technique

In the Y-factor technique, the noise figure is computed from two noise powers (N_c, N_h) measured with the noise source at its cold and hot temperatures (T_c, T_h) connected to the DUT. A second stage correction is necessary to eliminate the noise contribution of the receiver. To this end, a calibration step in which the receiver noise figure is characterized has to be performed. With the noise source directly connected to the receiver, two noise powers (N_{crec}, N_{hrec}) are measured. A basic block-diagram of measurement and calibration steps can be seen in Fig. 1. The DUT noise figure is computed as:

$$F_{YF} = F_{sys} - \frac{F_{rec}-1}{G_{ins}}, \tag{3}$$

where F_{sys} is the noise figure of the DUT-receiver system and F_{rec} is the receiver noise figure. Note that, in (3), G_{av} required by Friis formula [34] is approximated by the insertion gain of the DUT G_{ins}, computed from scalar measurements. Approximating the cold temperature T_c to the reference temperature of $T_o = 290$ K, these noise figures can be obtained as:

$$F_{sys} = \frac{(T_h/T_o - 1)}{N_h/N_c - 1}, \tag{4}$$

$$F_{rec} = \frac{(T_h/T_o - 1)}{N_{hrec}/N_{crec} - 1}. \tag{5}$$

G_{ins} is computed as:

$$G_{ins} = \frac{N_h - N_c}{N_{hrec} - N_{crec}}. \tag{6}$$

B) Cold-source technique

The cold-source technique computes the noise figure from a single noise measurement (N_{cs}) with a matched source load at room temperature T_c. For that, the available gain of the DUT and the gain-bandwidth product of the receiver ($\underline{kBG}_{rec}$) have to be previously determined. This $\underline{kBG}_{rec}$ term is usually obtained in the calibration step, required also for removing the noise contribution of the receiver. In cold-source technique, by definition, there is no hot measurement of the DUT. Thus, instead of G_{ins} the G_{av} computed from vector measurements is used. Since noise measurements are normally performed in a noise figure analyzer or a spectrum analyzer, obtaining G_{av} requires the additional use of a

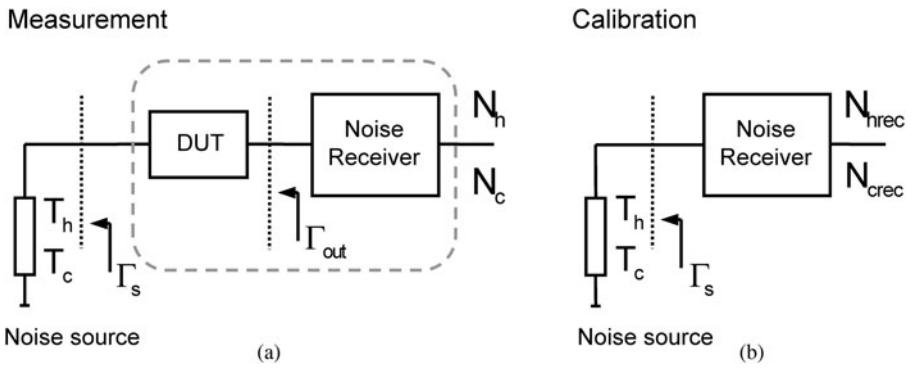

Fig. 1. Basic block-diagram of a Y-factor based noise figure measurement: (a) DUT measurement step; (b) calibration step.

https://doi.org/10.1017/S1759078713000688 Published online by Cambridge University Press

VNA. However, modern noise figure measurement capabilities included in VNA (PNA-X [25]) offer a significantly simplified vector corrected setup, especially valuable for the most challenging DUTs and setups [35, 36]. A basic block-diagram of cold-source based noise figure characterization is given in Fig. 2.

Thus, and considering $T_c \approx T_o$ again, the DUT noise figure can be characterized as in (7).

$$F_{CS} = F_{sysCS} - \frac{F_{rec} - 1}{G_{av}}, \tag{7}$$

where

$$F_{sysCS} = \frac{N_{cs}}{\underline{kBG}_{rec} G_{av} T_o}. \tag{8}$$

F_{rec} is, in its simplest form, that of (5) and

$$\underline{kBG}_{rec} = \frac{N_{hrec} - N_{crec}}{(T_h - T_c)}. \tag{9}$$

It is worthwhile to point out that (7)–(9) represent a simplified approach of the usual fully corrected cold-source implementation [18, 20] in which all mismatch terms have been neglected.

III. GENERAL EXPRESSIONS FOR NOISE FIGURE AS A FUNCTION OF SPOT NOISE FIGURE AND GAIN

In this section, the general expressions for Y-factor and cold-source techniques will be analytically formulated in terms of the spot noise figure and gain. For the sake of simplicity and to properly focus on the stated problem, any systematic effect apart from the influence of the measurement bandwidth will be neglected. In particular, a perfectly matched measurement path will be assumed and the cold temperature T_c will be approximated to the reference T_o.

Let us consider that the noise figure of a DUT with frequency dependent noise figure $F(f)$ and available gain $G(f)$ is to be characterized at a frequency f_o. Thus, the spot DUT noise figure $F(f_o) = F_{fo}$ is the desired result. For the characterization, a noise receiver with noise figure $F_{rec}(f)$ and transducer gain $G_{rec}(f)$ will be considered. Note that these $F_{rec}(f)$ and $G_{rec}(f)$ correspond to a bandpass type response, with a certain bandwidth B_{rec}, centered at f_o.

Since no mismatch will be present according to our approximation, there will be no difference between available and delivered noise powers. So from now on, $G(f)$ and $G_{rec}(f)$ will be simply referred to as gains.

A) Noise figure from Y-factor

The cold and hot noise powers (N_c, N_h) measured by the receiver in the DUT measurement step can be written as (10) and (11), respectively [26].

$$N_c = kT_o \int_o^\infty G_{rec}(f)\big(G(f)F(f) + \big(F_{rec}(f) - 1\big)\big)df, \tag{10}$$

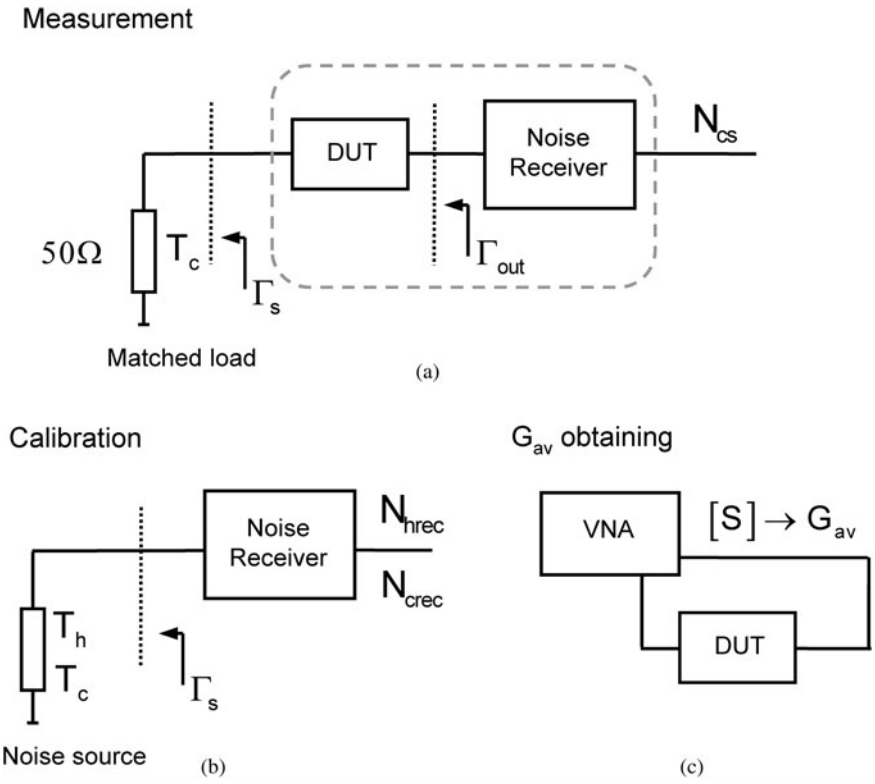

Fig. 2. Basic block-diagram of a cold-source based noise figure measurement: (a) DUT measurement step; (b) calibration step; (c) G_{av} obtaining.

https://doi.org/10.1017/S1759078713000688 Published online by Cambridge University Press

$$N_h = k\int_0^\infty G_{rec}(f)\big(T_h G(f) + T_0 G(f)\big(F(f)-1\big) + T_0\big(F_{rec}(f)-1\big)\big)df. \quad (11)$$

Besides, the cold and hot noise powers measured by the receiver in the calibration step can be written as in (12) and (13).

$$N_{crec} = kT_0\int_0^\infty G_{rec}(f)F_{rec}(f)df, \quad (12)$$

$$N_{hrec} = k\int_0^\infty \big(T_h G_{rec}(f) + T_0 G_{rec}(f)\big(F_{rec}(f)-1\big)\big)df. \quad (13)$$

In practice, the overall integrals in (10)–(13) are limited by the frequency selectivity of the two-ports involved.

Substituting (10) and (11) in (4), the system noise figure is given by:

$$F_{sys} = \frac{\int_0^\infty G_{rec}(f)\big(G(f)F(f) + \big(F_{rec}(f)-1\big)\big)df}{\int_0^\infty G_{rec}(f)G(f)df}. \quad (14)$$

Analogously, the receiver noise figure F_{rec} measured in the calibration step as in (5) leads to (15), which is the average receiver noise figure [37].

$$F_{rec} = \frac{\int_0^\infty G_{rec}(f)F_{rec}(f)df}{\int_0^\infty G_{rec}(f)df}. \quad (15)$$

The insertion gain obtained from (6) is also an average, weighted by the receiver gain, as shown in (16).

$$G_{ins} = \frac{\int_0^\infty G_{rec}(f)G(f)df}{\int_0^\infty G_{rec}(f)df}. \quad (16)$$

From (14) to (16), and applying (3), the resultant Y-factor noise figure is:

$$F_{YF} = \frac{\int_0^\infty G_{rec}(f)G(f)F(f)df}{\int_0^\infty G_{rec}(f)G(f)df}. \quad (17)$$

B) Noise figure from cold-source

In this case, the DUT noise figure will be computed by means of (7). With the assumptions made, i.e. no mismatch and $T_c \approx T_0$, N_{cs} comes to be N_c in (10). The computed gain-bandwidth product of the receiver will simply be:

$$\underline{kBG}_{rec} = k\int_0^\infty G_{rec}(f)df. \quad (18)$$

Besides, G_{av} in (7) and (8), computed from S-parameters, will be the spot gain corresponding to the measurement frequency f_0, i.e. $G_{av} = G(f_0) = G_{f0}$. Thus, the system noise figure characterized by means of cold-source will be:

$$F_{sysCS} = \frac{\int_0^\infty G_{rec}(f)\big(G(f)F(f) + \big(F_{rec}(f)-1\big)\big)df}{G_{f_0}\int_0^\infty G_{rec}(f)df}. \quad (19)$$

The noise figure obtained with cold-source is then:

$$F_{CS} = \frac{\int_0^\infty G_{rec}(f)G(f)F(f)df}{G_{f_0}\int_0^\infty G_{rec}(f)df}. \quad (20)$$

An important difference needs to be pointed out between (17) and (20). In (17), the integral in the denominator is limited to the actual bandwidth resulting from the series connection of the DUT and the receiver ($G_{rec}(f)G(f)$). On the contrary, in (20) the integral in the denominator is only limited by the receiver bandwidth $G_{rec}(f)$.

This difference has no relevance if the receiver bandwidth is narrower than the DUT, as will be the case of many conventional measurements. Actually, if we can consider that the DUT characteristics remain constant inside the receiver bandwidth, both (17) and (20) will yield the desired spot noise figure F_{f0}.

However, the difference between (17) and (20) can be significant when the DUT has a narrower bandwidth than the receiver. This situation is analyzed in detail in the following section.

IV. SYSTEM BANDWIDTH LIMITED BY THE DUT

Let us analyze here the case in which the bandwidth during the noise measurement is limited by the DUT instead of being restricted by the receiver. We can have this condition either because we are measuring ultra narrow-band DUTs, or because we want to speed up a measurement by choosing a wideband receiver. This situation is ideally sketched in Fig. 3(a). In addition, an equivalent situation happens when the measurement is performed in the pass-band edge of a DUT with a very sharp roll-off as depicted in Fig. 3(b).

To ease the derivation of qualitative conclusions, idealized band-pass frequency responses have been assigned to DUT and receiver in Fig. 3. DUT and receiver have constant gains (G_{f0} and $G_{orec,}$ respectively) inside their respective bandwidths (Fig. 3). In these conditions, the bandwidth during the measurement step will be given by the intersection of the DUT and receiver bandwidths. In the following, this system bandwidth will be notated as B_{sys}. A system bandwidth limited by the DUT implies that $B_{sys} < B_{rec}$.

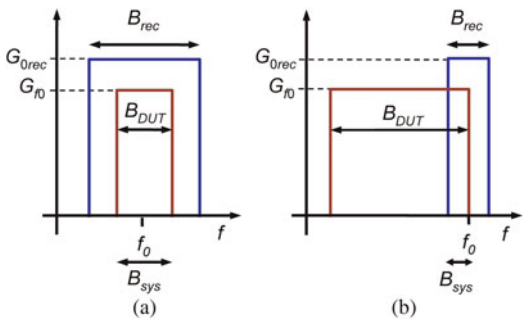

Fig. 3. Two possible sources of error: (a) DUT bandwidth narrower than receiver bandwidth; (b) measurement in DUT pass-band edge.

https://doi.org/10.1017/S1759078713000688 Published online by Cambridge University Press

Under these idealized conditions assumption, the available noise power density at the output of the DUT (N_{out}) for a source temperature T is that of (21). A basic diagram showing the noise behavior at the output of the DUT for the two situations of Fig. 3 is given in Fig. 4.

$$N_{out}(f) = kG(f)\left(T + T_o\left(F(f) - 1\right)\right) \approx \begin{cases} kG_{fo}\left(T + T_o\left(F_{fo} - 1\right)\right) & f \in B_{DUT} \\ kT_o & f \notin B_{DUT} \end{cases}. \quad (21)$$

A) Impact of $B_{sys} < B_{rec}$ on Y-factor

From (21), the measured cold and hot noise powers, (10) and (11) can be rewritten as (22) and (23), respectively:

$$N_c \approx kG_{orec}\left[B_{sys}G_{fo}F_{fo}T_o + \left(B_{rec} - B_{sys}\right)T_o + B_{rec}T_o(F_{rec} - 1)\right], \quad (22)$$

$$N_h \approx kG_{orec}\left[B_{sys}G_{f_o}\left(T_h + T_o\left(F_{f_o} - 1\right)\right) + \left(B_{rec} - B_{sys}\right)T_o + B_{rec}T_o(F_{rec} - 1)\right], \quad (23)$$

where $kG_{orec}(B_{rec} - B_{sys})T_o$ is the out-of-band noise contribution of the DUT inside B_{rec}.

Let us reconsider the Y-factor formulation under the assumptions made. From these noise powers (22), (23) the system noise figure (14) results in:

$$F_{sys} \approx F_{f_o} + \left(\frac{B_{rec}}{B_{sys}} - 1\right)\frac{1}{G_{f_o}} + \frac{B_{rec}}{B_{sys}}\frac{(F_{rec} - 1)}{G_{f_o}}, \quad (24)$$

which agrees with [32]. Besides, the insertion gain (16) will turn into:

$$G_{ins} \approx \frac{B_{sys}}{B_{rec}}G_{f_o}. \quad (25)$$

Thus, the DUT noise figure characterized by means of Y-factor will be:

$$F_{YF} \approx F_{f_o} + \left(\frac{B_{rec}}{B_{sys}} - 1\right)\frac{1}{G_{f_o}}. \quad (26)$$

It is commonly accepted, [28, 29], that the error due to $B_{sys} < B_{rec}$ in Y-factor comes from the extra noise detected in the calibration step. However, as it can be concluded from (22)–(26), the error comes from the out-of-band noise contribution of the DUT during the measurement step (the term $kG_{orec}(B_{rec} - B_{sys})T_o$), as pointed-out in [32]. Besides, the error for a given B_{sys} decreases as G_{fo} increases, turning negligible for a G_{fo} significantly higher than the $(B_{rec} - B_{sys})/B_{sys}$ ratio. In other words, the error turns negligible for a gain high enough to make the out of band noise contribution of the DUT negligible. It should be noted in (26) that the result is not an underestimation of the DUT noise figure, as concluded from [28] or stated in [29], but an overestimation [31, 32].

B) Impact of $B_{sys} < B_{rec}$ on cold-source

Coming to cold-source, N_{cs} is again approximated by (22), so (19) leads to:

$$F_{sysCS} \approx F_{f_o}\frac{B_{sys}}{B_{rec}} + \left(1 - \frac{B_{sys}}{B_{rec}}\right)\frac{1}{G_{f_o}} + \frac{(F_{rec} - 1)}{G_{f_o}}. \quad (27)$$

Thus, the cold-source noise figure result is:

$$F_{CS} \approx F_{f_o}\frac{B_{sys}}{B_{rec}} + \left(1 - \frac{B_{sys}}{B_{rec}}\right)\frac{1}{G_{f_o}}. \quad (28)$$

There is a substantial difference between this result and the previous Y-factor (26). In Y-factor the error tends to disappear as DUT gain increases, however, this is not the case for cold-source. Actually, the error, in dB, tends to the bandwidth ratio $(B_{sys}/B_{rec})_{dB}$ for a significant DUT gain that makes negligible the second term in (28). This comes directly from the fact that the integral in the denominator of (20) is limited by the receiver (B_{rec}) while the integral in the numerator is limited by the series connection of DUT and receiver (B_{sys}). This ratio makes the first term in (28) to underestimate the spot noise figure, for any DUT gain.

V. CORRECTION TERMS

In sight of the previous results, correction terms can be estimated, for both cold-source and Y-factor, to minimize the effect of a system bandwidth limited by the DUT. To this

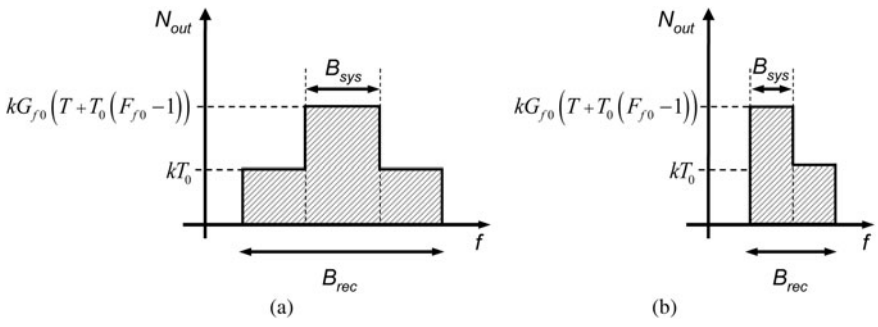

Fig. 4. Noise power density available at the output of the DUT within the receiver bandwidth: (a) DUT bandwidth narrower than receiver bandwidth; (b) measurement in DUT pass-band edge.

https://doi.org/10.1017/S1759078713000688 Published online by Cambridge University Press

end, the knowledge of the bandwidth ratio B_{sys}/B_{rec} would be required. It is important to note that these corrections are approximate because they rely on the ideal band-pass characteristics of DUT and receiver.

A) Y-factor

In Y-factor, according to (25), the B_{sys}/B_{rec} ratio can be estimated from (29).

$$\frac{B_{sys}}{B_{rec}} \approx \frac{G_{ins}}{G_{f_o}}. \tag{29}$$

G_{ins} is known from the Y-factor measurement while G_{f0} can be determined from an additional measurement with a vector network analyzer, for instance. The corrected Y-factor expression would then be:

$$F_{YF\_corr} = F_{YF} - \left(\frac{1}{G_{ins}/G_{f_o}} - 1\right)\frac{1}{G_{f_o}}. \tag{30}$$

B) Cold-source

In cold-source the insertion gain G_{ins} is not known. Therefore (29) cannot be used to estimate the B_{sys}/B_{rec} ratio. However, a fair approximation to B_{sys}/B_{rec} can be achieved as:

$$\frac{B_{sys}}{B_{rec}} \approx \frac{\overline{G(f)}\Big|_{B_{rec}}}{G_{f_o}}, \tag{31}$$

where $\overline{G(f)}\Big|_{B_{rec}}$ is the average gain of the DUT in the receiver bandwidth. This average gain can be obtained from an S-parameter characterization of the DUT in the whole B_{rec}. It is important to remember that (31) is only an approximation because B_{rec} is assumed to have an ideal rectangular band-pass frequency-response. According to (28) and (31), the corrected cold-source result can be calculated as:

$$F_{CS\_corr} = F_{CS}\frac{1}{\overline{G(f)}\Big|_{B_{rec}}/G_{f_o}} - \left(\frac{1}{\overline{G(f)}\Big|_{B_{rec}}/G_{f_o}} - 1\right)\frac{1}{G_{f_o}}. \tag{32}$$

VI. MEASUREMENTS

To verify the validity of the analysis and formulation presented in this paper, relevant measurement results are provided. The noise measurements have been performed in a spectrum analyzer including noise figure measurement capabilities (PSA E4440), with a 346B noise source. A PNA E8358A has been used for vector measurements.

For the measurements, three DUTs (labeled as DUT1, DUT2, and DUT3) with different gains and a 3 dB bandwidth of approximately 2 MHz, are considered. The DUTs are in-home built, cascading packaged commercial amplifiers and narrow-band filters. Attenuators at the output avoid mismatch effects, eliminating the necessity of a full noise receiver calibration. It is important to note that the whole analysis has been developed on the basis of a matched setup. Taking into account mismatch effects would require a rigorous analysis of the overall effects on the obtained results and their correction, as well as requiring more demanding measurement setups. This can be the case, for instance, of on-wafer noise characterization, where the effect of input/output access blocks has to be removed [38–41].

A) Gain and noise characteristics of the DUTs versus frequency

Figures 5 and 6 show, respectively, the spot gains and noise figures of the DUTs as a function of frequency in a 6 MHz range centered at 70 MHz. The gains have been computed from vector measurements in the PNA. The noise figures have been characterized by means of cold-source technique, from noise measurements carried out in the PSA with a bandwidth of 51 kHz at each measurement point. The three DUTs present equal spot noise figure (6.25 dB) while different spot gains (4, 6.75 and 20.5 dB, respectively) at 70 MHz. These values are taken as the reference true values for the rest of the analysis.

B) Noise figure measurements with different receiver bandwidths

First, the evolution of Y-factor and cold-source noise figure measurement results for increasing receiver bandwidth has been analyzed. For that, the noise figure of DUT1 has been measured at its central frequency of 70 MHz with five different receiver bandwidth settings (0.51, 1, 2, 4, and 6 MHz). These receiver bandwidths lead approximately to the following B_{sys}/B_{rec} ratios, respectively: 0.99, 0.96, 0.84, 0.57 and 0.38. According to (29), these values can be estimated dividing the insertion gain computed in each measurement with the spot insertion gain.

Y-factor and cold-source noise figures (labeled as F_{YF} and F_{CS}, respectively) have been measured as described in Section II. The measurement results, given in Fig. 7, clearly show how the accuracy degrades as the receiver

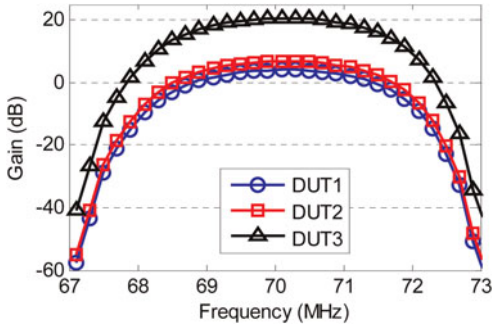

Fig. 5. Spot gains of the three DUTs in the 67–73-MHz frequency range.

https://doi.org/10.1017/S1759078713000688 Published online by Cambridge University Press

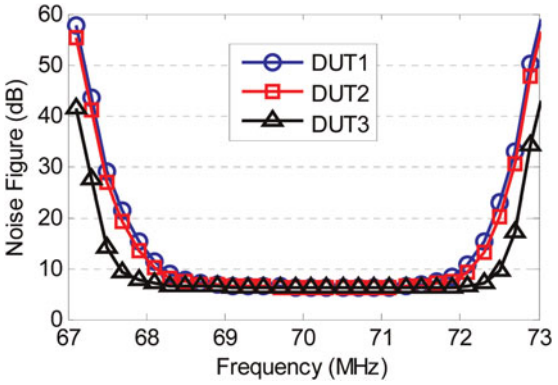

Fig. 6. Spot noise figures of the three DUTs in the 67–73-MHz frequency range.

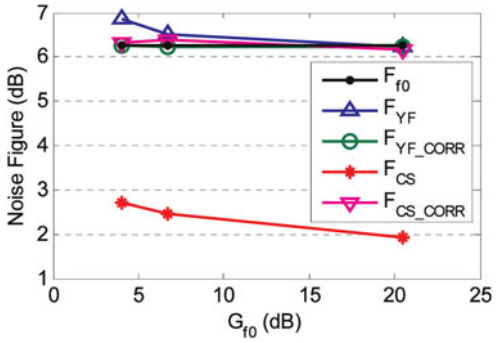

Fig. 8. Y-factor and cold-source noise figures of the three DUTs measured with $B_{rec} = 6$ MHz (with and without corrections), and comparison to the actual spot noise figure $F_{fo} = 6.25$ dB.

bandwidth widens. Results confirm that Y-factor overestimates the actual DUT noise figure (approximately 0.6 dB for a B_{rec} of 6 MHz), as pointed out in Section IV. In contrast, the cold-source results are significantly less accurate than Y-factor and below the true DUT noise figure. With a B_{rec} of 6 MHz the noise figure obtained from cold-source technique is more than 3 dB lower than the true value.

C) Noise figure measurements as a function of DUT gain and correction terms

Let us now verify the effect of DUT gain on the measurement results. For that, the Y-factor and cold-source noise figures of the three DUTs have been measured at 70 MHz setting B_{rec} to 6 MHz. In addition, their corrected versions (30) and (32) have been computed. For the sake of clarity, the results have been depicted in Fig. 8 as a function of DUT gain. The results shown in Fig. 8 are in very good agreement with the conclusions presented in Section IV. When coming to Y-factor, as expected, the error disappears for high DUT gain. However, in cold-source the error augments as DUT gain increases. The worst case is an underestimation of approximately 4.2 dB for DUT3, i.e. for highest gain. As expected from (28), this error is $(B_{sys}/B_{rec})_{dB}$.

Finally, let us analyze the correction terms proposed in Section V. As it can be seen in Fig. 8, the errors are almost eliminated with the corrected versions (F_{YF_corr} and F_{CS_corr}) even though they are based on ideally rectangular band-pass frequency responses. These results show that the correction terms can be an acceptable solution when receivers with narrow bandwidth are not either available or recommended (because we may be interested in speeding up the measurement process, for instance).

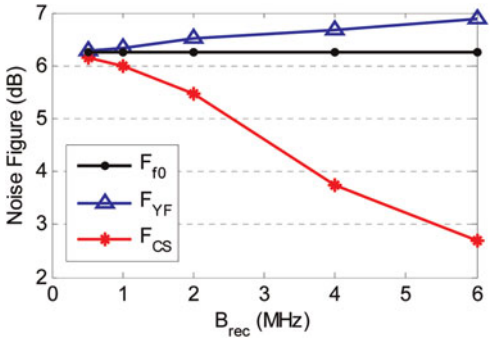

Fig. 7. Y-factor (F_{YF}) and cold-source (F_{CS}) noise figure measurements of DUT1 with five receiver bandwidths compared to the actual spot noise figure $F_{fo} = 6.25$ dB.

VII. CONCLUSION

The effect of receiver bandwidth on Y-factor and cold-source noise figure measurements has been analyzed and compared. Results show that, contrary to Y-factor, errors associated with a wide receiver bandwidth in cold-source increase with DUT gain and generate a critical underestimation of the actual noise figure. As a consequence, the use of wide receiver bandwidths to speed up the measurement process in high gain DUTs, acceptable in Y-factor, should be avoided in cold-source. Bandwidth selection has to be carefully considered when measuring noise figure with cold-source technique, especially in ultra narrow-band DUTs or at the band-pass edge of DUTs with sharp roll-offs. Nonetheless, the availability of receivers with narrow enough bandwidths for accurate narrow-band DUT characterization may be limited by the capabilities of the measurement instrument. Correction terms have then been proposed to improve accuracy when narrow-band receivers are not available. Conclusions of the analysis have been experimentally validated by means of noise measurements performed on various narrow-band DUTs with different characteristics.

ACKNOWLEDGEMENT

This work was supported in part by Spanish and Basque administrations, respectively, under Project TEC2012-35875 and Project IT456-10.

REFERENCES

[1] Randa, J.; Dunsmore, J.; Dazhen, G., Wong, K., Walker, D.K.; Pollard, R.D.: Verification of noise-parameter measurements and uncertainties. IEEE Trans. Instrum. Meas., **60** (11) (2011), 3685–3693.

https://doi.org/10.1017/S1759078713000688 Published online by Cambridge University Press

[2] Kerr, A.R.; Randa, J.: Thermal noise and noise measurements – A 2010 update. Microw. Mag., **11** (6) (2010), 40–52.

[3] Garelli, M.; Ferrero, A.; Bonino, S.: A complete noise- and scattering-parameters test-set. IEEE Trans. Microw. Theory Tech., **57** (3) (2009), 716–724.

[4] Pasquet, D.; Bourdel, E.; Quintanel, S.; Ravalet, T.; Houssin, P.: New method for noise-parameter measurement of a mismatched linear two-port using noise power wave formalism. IEEE Trans. Microw. Theory Tech., **56** (9) (2008), 2136–2142.

[5] Otegi, N.; Collantes, J.M.; Sayed, M.: Cold-source measurements for noise figure calculation in spectrum analyzers, in 67th ARFTG Conf. Digest, June 2006, 223–228.

[6] Tiemeijer, L.F.; Havens, R.J.; de Kort, R.; Scholten, A.J.: Improved Y-factor method for wide-band on-wafer noise parameter measurements. IEEE Trans. Microw. Theory Tech., **53** (9) (2005), 2917–2925.

[7] Weatherspoon, M.; Dunleavy, L.: Vector corrected on-wafer measurements of noise temperature. IEEE Trans. Instrum. Meas., **54** (3) (2005), 1327–1332.

[8] Wiatr, W.; Walker, D.K.: Systematic errors of noise parameter determination caused by imperfect source impedance measurement. IEEE Trans. Instrum. Meas., **54** (2) (2005), 696–700.

[9] Collantes, J.M.; Pollard, R.D.; Sayed, M.: Effects of DUT mismatch on the noise figure characterization: a comparative analysis of two Y-factor techniques. IEEE Trans. Instrum. Meas., **51** (6) (2002), 1150–1156.

[10] Vondran, D.: Noise figure measurement: corrections related to match and gain. Microw. J., **42** (1999), 22–38.

[11] Lazaro, A.; Pradell, L.; O'Callaghan, J.M.: Method for measuring noise parameters of microwave two-port. Electron. Lett., **34** (13) (1998), 1332–1333.

[12] Crozat, P.; Boutez, C.; Chaubet, M.; Danelon, V.; Sylvestre, A.; Vernet, G.: 50 W noise measurements with full receiver calibration without tuner. Electron. Lett., **32** (3) (1996), 261–262.

[13] Valk, E.; Johansen, H.C.; Routledge, D.; Vaneldik, J.F.; Landecker, T.L.: Improving accuracy of microwave noise measurements of highly mismatched devices. Electron. Lett., **28** (22) (1992), 2035–2037.

[14] Agilent N8973A, N8974A, N8975A NFA Series Noise Figure Analyzers. Agilent Data Sheet 5980-0164E, November 2007.

[15] Agilent PSA Series Spectrum Analyzers. Noise Figure Measurements Personality. Agilent Technical Overview 5988-7884EN, August 2005.

[16] Noise Figure, Scorpion Option 4. Anritsu Application Note 11410-00210, April 2000.

[17] Adamian, V.; Uhlir, A.: A novel procedure for receiver noise characterization. IEEE Trans. Instrum. Meas., **22** (2) (1973), 181–182.

[18] Davidson, A.C.; Leake, B.W.; Strid, E.: Accuracy improvements in microwave noise parameter measurements. IEEE Trans. Microw. Theory Tech., **37** (12) (1989), 1973–1978.

[19] Meierer, R.; Tsironis, C.: An on-wafer noise parameter measurement technique with automatic receiver calibration. Microw. J., **38** (1995), 22–37.

[20] Otegi, N.; Collantes, J.M.; Sayed, M.: Receiver noise calibration for a vector network analyzer, in 76th ARFTG Conf. Digest, December 2010, 1–5.

[21] Escotte, L.; Plana, R.; Graffeuil, J.: Evaluation of noise parameter extraction methods. IEEE Trans. Microw. Theory Tech., **41** (3) (1993), 382–387.

[22] Ballo, D.: Making source-corrected noise-figure measurements. Microw. RF, **46** (9) (2007), 1.

[23] Anritsu Co.: VNAs measure noise from 70 kHz to 125 GHz. Microw. RF, **51** (7) (2012), 84.

[24] IRE standards on methods of measuring noise in linear twoports, 1959. Proc. IRE, **48** (1) (1960), 60–68.

[25] Agilent 2-Port and 4-Port PNA-X Network Analyzer. Agilent Data Sheet N5242-90007, April 2009.

[26] Carlson, A.B.: Communication Systems, 3rd ed., McGraw-Hill, Boston, 1986.

[27] Rudolph, M.; Heymann, P.; Boss, H.: Impact of receiver bandwidth and nonlinearity on noise measurements methods. Microw. Mag., **11** (6), (2010), 110–121.

[28] Noise Figure Measurement Accuracy – The Y-Factor Method. Agilent Application Note 57-2, May 2010.

[29] 10 Hints for Making Successful Noise Figure Measurements. Agilent Application Note 57-3, November 2011.

[30] Noise Figure Corrections. Anritsu Application Note 11410-00256, November 2000.

[31] Practical Noise Figure-Measurement and Analysis for Low-Noise Amplifier Designs. Agilent Application Note 1354, September 2000.

[32] Pastori, W.E.: Bandwidth effects in noise figure measurements. 29th ARFTG Conf. Digest-Spring, **11** (1987), 1–16.

[33] Fundamentals of RF and Microwave Noise Figure Measurements. Agilent Application Note 57-1, October 2000.

[34] Friis, H.T.: Noise figure of radio receivers. Proc. IRE, **32** (7) (1944), 419–422.

[35] Simpson, G.M.; Ballo, D.J.; Dunsmore, J.P.; Ganwani, A.: A new noise parameter measurement method results in more than 100× speed improvement and enhanced measurement accuracy, in 72nd ARFTG Conf. Digest, December 2008, 119–127.

[36] Wiatr, W.; Crupi, G.; Caddemi, A.; Mercha, A.; Schreurs, D.M.M.-P.: Source-pull characterization of FinFET noise, in Proc. of the 17th Int. Conf. on Mixed Design of Integrated Circuits and Systems MIXDES 2010, June 2010, 425–430.

[37] Description of the noise performance of amplifiers and receiving systems. Proc. IRE, **51** (3) (1963), 436–442.

[38] Gao, J.; Law, C.L.; Wang, H.; Aditya, S.; Boeck, G.: A new method for pHEMT noise-parameter determination based on 50-Ω noise measurement system. IEEE Trans. Microw. Theory Tech., **51** (10) (2003), 2079–2089.

[39] Lazaro, A.; Pradell, L.; O' Callaghan, J.M.: FET noise-parameter determination using a novel technique based on a 50-W noise-figure measurements. IEEE Trans. Microw. Theory Tech., **47** (1999), 315–324.

[40] Tasker, P.J.; Reinert, W.; Hughes, B.; Braunstein, J.; Schlechtweg, M.: Transistor noise parameter extraction using a 50-Ω measurement system, in IEEE MTT-S Int. Microwave Symp. (IMS) Digest, June 1993, 1251–1254.

[41] Dambrine, G.; Happy, H.; Danneville, F.; Cappy, A.: A new method for on wafer noise measurement. IEEE Trans. Microw. Theory Tech., **41** (3) (1993), 375–381.

https://doi.org/10.1017/S1759078713000688 Published online by Cambridge University Press

Nerea Otegi received the Ph.D. degree from the University of the Basque Country (UPV/EHU), Bilbao, Spain, in 2008. In 2002, she joined the Electricity and Electronics Department, UPV/EHU, where she has been an Associate Professor since 2006. Her areas of interest include noise characterization at microwave frequencies and nonlinear analysis of microwave circuits.

Juan-Mari Collantes received the Ph.D. degree in electronics from the University of Limoges, France, in 1996. Since February 1996, he has been an Associate Professor with the Electricity and Electronics Department, University of the Basque Country (UPV/EHU), Bilbao, Spain. In 1996 and 1998, he was an Invited Researcher with Agilent Technologies (formerly the Hewlett-Packard Company), Santa Rosa, CA. In 2003, he was with the French Space Agency (CNES), Toulouse, France, where he was involved with power amplifier analysis, simulation, and modeling. His areas of interest include nonlinear analysis and design of microwave circuits, microwave measurement techniques, and noise characterization.

Mohamed Sayed received BS and MS degrees in electrical engineering, from Cairo University, Egypt. He earned his Ph.D. degree in electrical engineering from Johns Hopkins University, Baltimore, Maryland. Mohamed is currently principal consultant for Microwave and Millimeter Wave Solutions. He previously worked at Hewlett-Packard and Agilent Technologies for 30 years. He is a world-wide expert on microwave and millimeter wave products and systems. He developed and launched state-of-the-art technologies for vector network analyzers, sources, and spectrum analyzers. Mohamed is an IEEE Life Senior Member. He is currently the ARFTG Vice President, and was general and technical program chair for several ARFTG conferences. He is also on the steering committee of the IEEE Wireless and Microwave Technology Conference. Mohamed is the author and co-author of over 70 publications on device characterization, microwave and millimeter wave measurement systems, and high power amplifier design. He also reviews technical papers for ARFTG conferences and IEEE publications.

https://doi.org/10.1017/S1759078713000688 Published online by Cambridge University Press